Investigation on Compressed Wavefront Sensing in Freeform Surface Measurements

Eddy Chow Mun Tik[1], Xin Wang[1] , Ningqun Guo[1], Ching SeongTan[2] and Kuew Wai Chew[3]
[1]*School of Engineering, Monash University Malaysia, Jalan Lagoon Selatan, Bandar Sunway, Subang Jaya, Malaysia*
[2]*Faculty of Engineering, Multimedia University, Cyberjaya, Malaysia*
[3]*Faculty of Engineering and Science, University Tunku Abdul Rahman, Kampar, Malasyia*

Shack-Hartmann Wavefront Sensing, Compressed Sensing, Freeform Surface Measurement.

Abstract: In this paper, conventional modal wavefront reconstruction is compared with compressed wavefront sensing to reconstruct freeform surface profiles using the Shack-Hartmann wavefront sensor. The modal wavefront reconstruction represents the phase or the wavefront in the Zernike domain. The compressed wavefront sensing method based on the sparse Zernike representation (SPARZER) represents the phase slopes in the Zernike domain. The effectiveness of compressed wavefront sensing in freeform surface profile measurements is investigated.

1 INTRODUCTION

The Shack-Hartmann wavefront sensor has been popular due to its simplicity in measuring the shape of a wavefront. Since the start of its development in the late 1960s for the use of improving images captured from ground telescopes (Platt & Shack, 2001), its applications expanded to measurement of aberrations of the eye and optical component characterization among others (Schwiegerling & Neal, 2005). There have been a great amount of research to improve the accuracy of the Shack-Hartmann wavefront sensor. This includes new centroid detection algorithms (Yin, et al., 2009), de-noising centroid images (Basden, et al., 2015), use of new basis functions (Lundstrom & Unsbo, 2004), and new wavefront reconstruction algorithms (Rostami, et al., 2012).

Compressive sensing meanwhile is a great optimization technique to recover sparse signals even when the sampling rate is lower than required by the Shannon-Nyquist sampling theorem (Donoho, 2006). This is done by solving underdetermined linear systems where the signal is sparse in a particular domain. Another requirement is the incoherence between the sampling and the representing domains e.g. the time and frequency domains (Candes & Romberg, 2005). The linear equations are solved using l1 minimization, which does not have an analytical solution. It is solved using iterative numerical methods such as linear programming etc. (Candes, et al., 2006)

Application of compressed sensing on the Shack-Hartmann wavefront sensor is possible because there exist a sparse representation of the projected wavefront. A popular representation of the wavefront is in the Zernike domain (Noll, 1976). Early work has shown different implementations of compressive sensing in Shack-Hartmann wavefront sensors. This includes the representation of phase slopes in the Zernike domain (Polans, et al., 2014), and defining the sensing domain as the Dirac comb (Hosseini & Michailovich, 2009).

The use of Shack-Hartmann wavefront sensing on free-form surfaces presents some challenges due to the nature of freeform surfaces themselves. Due to large slopes or curvature of freeform surfaces, the focal spot on the image sensor could be distorted (Guo, et al., 2013). This causes the centroid detection algorithm to be inaccurate, and thus producing inaccurate phase slope measurements. Compressive wavefront sensing has shown to reconstruct wavefronts accurately even with noisy measurements (Polans, et al., 2014).

Tik, E., Wang, X., Guo, N., SeongTan, C. and Chew, K.
Investigation on Compressed Wavefront Sensing in Freeform Surface Measurements.
DOI: 10.5220/0005743901520157
In *Proceedings of the 4th International Conference on Photonics, Optics and Laser Technology (PHOTOPTICS 2016)*, pages 154-159
ISBN: 978-989-758-174-8

2 THEORY

2.1 Modal Wavefront Reconstruction

The classic modal reconstruction of Shack-Hartmann wavefront sensors uses the least squares optimization to solve the linear equations which approximate the wavefront to a summation of some decomposed polynomials (Dai, 1994).

$$\phi = \sum_{i=1}^{\infty} a_i Z_i \quad (1)$$

Where a_i is the ith coefficient, and Z_i is the ith polynomial. The commonly used polynomials are the Zernike polynomials and Fourier transforms.

The information obtained from the Shack-Hartmann wavefront sensor meanwhile are the phase slopes in the x and y direction of phase Φ, which can be approximated to the distance of a focal spot to its reference divided by the focal length of the lenslets.

$$\frac{\partial \phi}{\partial x} = \frac{\Delta x}{f} = f_x \quad (2)$$

$$\frac{\partial \phi}{\partial y} = \frac{\Delta y}{f} = f_y \quad (3)$$

For a Shack-Hartmann wavefront sensor with lenslets of n×n grid, the number of phase slope measurements will be $2n^2$. In matrix form, the above equations can be represented as

$$\boldsymbol{F = EA} \quad (4)$$

Where F is the column matrix of phase slope measurements, E is matrix of the partial differentials of polynomials Z in the x and y direction, and A is the matrix of coefficients of Z.

The elements in matrix E, are the average Zernike derivatives over the corresponding sub-apertures of the Shack-Hartmann wavefront sensor.

The least squares solution to the above equation would be

$$\boldsymbol{A = (E^T E)^{-1} E^T F} \quad (5)$$

2.2 Compressed Wavefront Sensing

The method used for compressed wavefront sensing is the sparse Zernike representation (SPARZER). SPARZER is a method proposed by James Polans where the phase slopes itself are represented using Zernike polynomials (Polans, et al., 2014). Due to the condition where the phase map has to be continuously differentiable in the Zernike space, implementation of this technique is simpler. First, the phase slopes are represented in the Zernike orthonormal basis.

$$\frac{\partial \phi}{\partial x} = f_x = Z c_x \quad (6)$$

$$\frac{\partial \phi}{\partial y} = f_y = Z c_y \quad (7)$$

c_x and c_y are the coefficients in the Zernike domain while Z is the matrix transforming the slope information into the Zernike domain across the entire phase map. The amount of phase slope information is then compressed by randomly selecting a set percentage of the slope data. Then, using this limited amount of information, SPARZER reconstructs the sparse signal in the Zernike domain using the equation

$$c' = argmin\left\{\frac{1}{2}\|\psi Z c - b\|_2^2 + \lambda \|c\|_1\right\} \quad (7)$$

In equation 7, c is the matrix of coefficients in the Zernike domain, b is the phase slope measurements, and ψ is the sparse sampling operator.

While in his paper, Polans uses randomised samples from a set of slope data from high lenslet density (HLD) array, this investigation uses samples similar to the shape of Shack-Hartmann lenslet arrays with lower density to reconstruct the signal.

3 SIMULATION RESULTS

Five different lenslet sizes are used in this simulation. The number of lenslets for each case are 317, 197, 149, 113 and 81 respectively. The simulated reference focal spot image for the highest and lowest number of lenslets are shown in Figure 1.

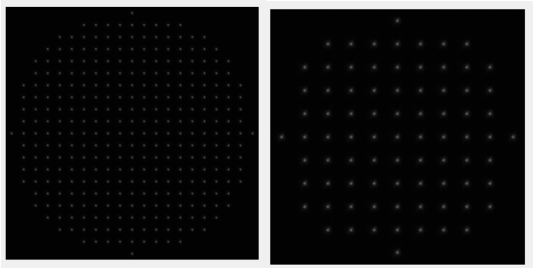

Figure 1: Reference focal spot images.

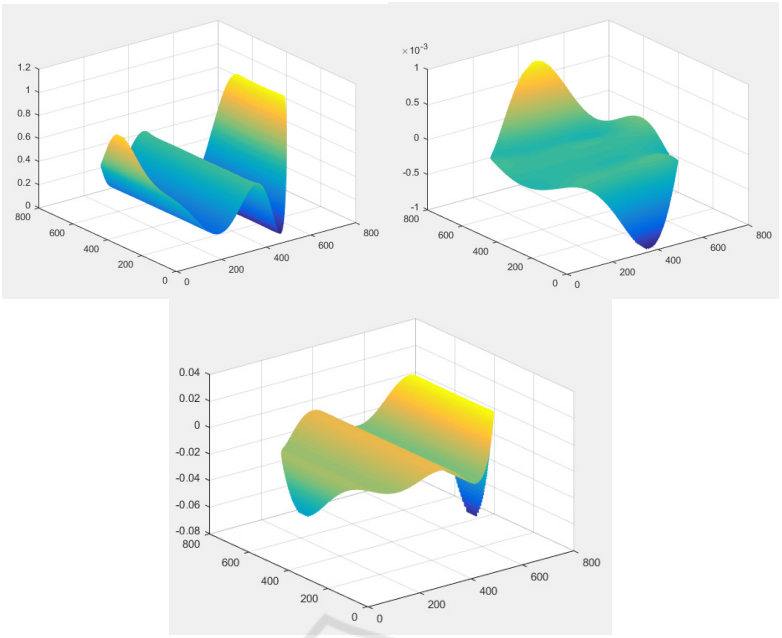

Figure 2: from left: a) test freeform wavefront b) x-slope of wavefront and c) y-slope of wavefront.

The simulation is run using a test freeform wavefront shown in Figure 2. The test wavefront has various peaks and valleys and a region of large phase slope. This would be able to test out and compare both reconstruction techniques.

The conventional modal wavefront reconstruction reconstructs the test wavefront relatively well for all cases. For the case of 317 lenslets, it can be seen that the reconstructed wavefront retains the overall profile of the test wavefront from Figure 3. The maximum error of the reconstructed wavefront is 0.13 microns. Figure 4 shows the overall absolute error across the entire phase map.

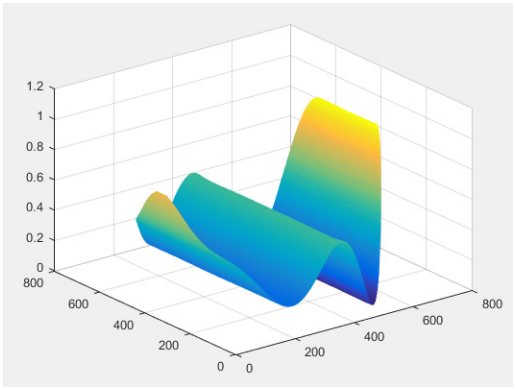

Figure 3: Reconstructed wavefront using conventional modal reconstruction (317 lenslet).

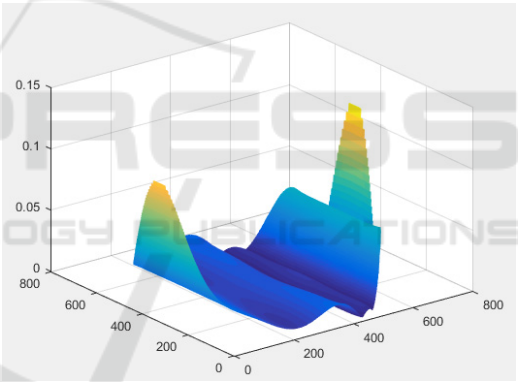

Figure 4: Absolute error (in microns).

It can be seen that the highest amount of error is in the peak region near both ends of the wavefront, and the lowest valley on the right. The wavefront was reconstructed using 36 Zernike polynomials. Due to the limited amount of higher order polynomials, and the edge being the highest point of the wavefront, the peak could not be resolved accurately. This occurs for all the different number of lenslet used. This shows the limitation in representing phase in the Zernike domain. Low order Zernike polynomials are very smooth and are unstable at the outer regions (Dalal, et al., 2001). Thus they are not very suitable for freeform wavefronts.

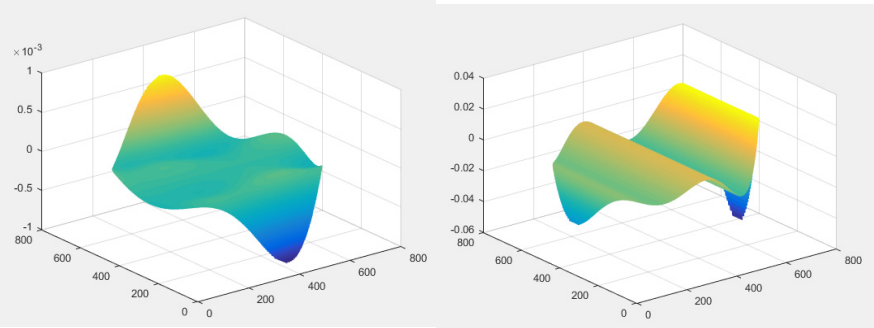

Figure 5: x and y slopes from the reconstructed wavefront.

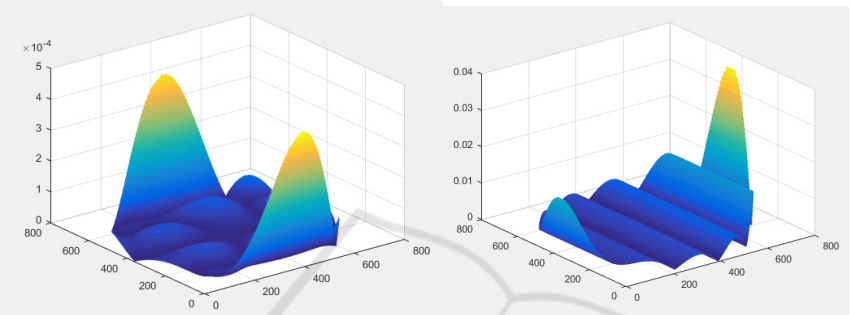

Figure 6: Absolute error of x and y slopes.

The x and y slopes calculated from the reconstructed wavefront are shown in Figure 5 and their error in Figure 6. Again, it can be seen that the edges have a higher error which is caused by the inaccuracies in the edges of the reconstructed wavefront. Discounting the peak at the edges, the mean error for the x and y slopes are 2.575×10^{-5} and 2.649×10^{-3} respectively.

SPARZER meanwhile reconstructs the slopes of the wavefront. The reconstructed slopes using 317 lenslets are shown in Figure 7 and 8, while the absolute error of the reconstructed slopes are in Figure 9. Similar to the slope errors from the modal reconstruction, the largest errors are at the edges where the slopes are larger in value. Discounting the peak values at the edges, the mean error for x and y slopes reconstructed are 2.6346×10^{-6} and 2.042×10^{-4} respectively.

Table 1 shows the mean error of x and y slopes obtained using compressed sensing and modal reconstruction. From the table, it can be seen that compressed sensing has a lower mean error when compared to modal reconstruction for all cases.

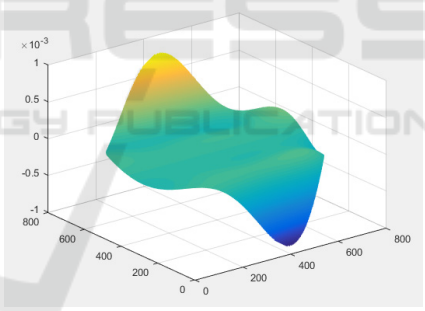

Figure 7: x-slope reconstructed with SPARZER.

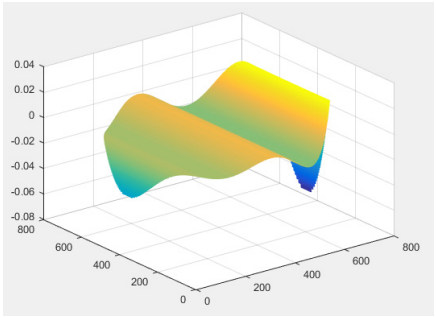

Figure 8: y-slope reconstructed with SPARZER.

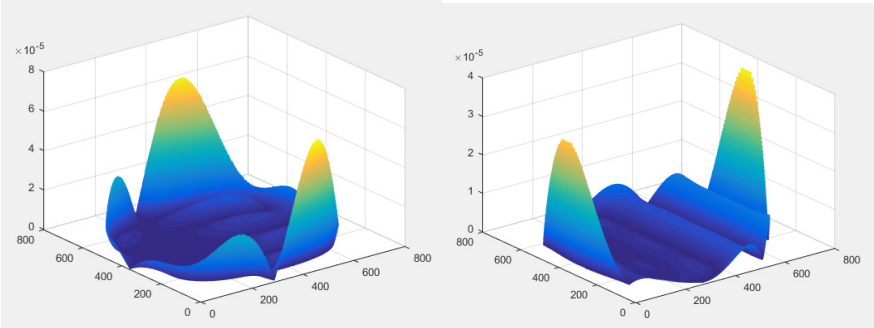

Figure 9: Absolute error of x and y slopes reconstructed with SPARZER.

Table 1: Mean error of wavefront slopes.

No. lenslets	mean error for compressed sensing		mean error for modal reconstruction	
	x-slope	y-slope	x-slope	y-slope
317	2.63×10^{-6}	2.04×10^{-6}	4.12×10^{-5}	5.21×10^{-3}
197	8.59×10^{-6}	3.53×10^{-6}	4.18×10^{-5}	5.24×10^{-3}
149	9.84×10^{-6}	1.09×10^{-5}	4.21×10^{-5}	5.26×10^{-3}
113	1.31×10^{-5}	1.30×10^{-4}	4.21×10^{-5}	5.26×10^{-3}
81	2.43×10^{-5}	5.68×10^{-4}	4.20×10^{-5}	5.25×10^{-3}

Besides that, the mean error for compressed sensing when using the lowest number of lenslet is lower than the mean error for all cases using modal reconstruction. The error from compressed sensing follows the trend where the higher the number of samples, the lower the error. Meanwhile for modal reconstruction, the error stays relatively constant.

However, while the mean errors are lower, the slopes reconstructed using 81 lenslets do not match well with the original slopes visually. Shown in Figure 10 are the slopes reconstructed using 81 lenslets.

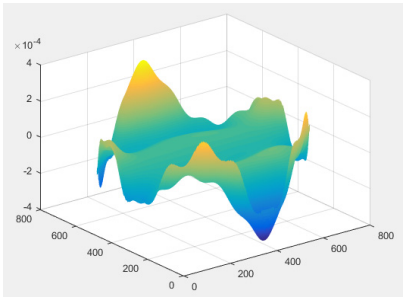

Figure 10: x-slope reconstructed with SPARZER.

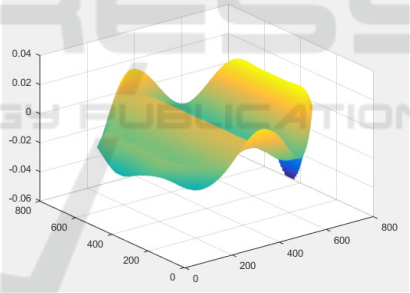

Figure 11: y-slope reconstructed with SPARZER.

The profile at the edges deviate the most when compared to the original slopes of the wavefront. This is again due to the limitations of Zernike polynomials in freeform surface measurements.

4 CONCLUSIONS

It can be seen that at lower lenslet resolutions, there are large deviations in the edges of the slopes reconstructed by compressed sensing. This is caused by the inability of Zernike polynomials to accurately represent freeform surface profiles. Similarly, for modal wavefront reconstruction, the error is also highest at the edges of the wavefront. However, it is

clear that compressed sensing yields a lower error when compared to modal reconstruction for all lenslet resolutions.

ACKNOWLEDGEMENT

The authors gratefully acknowledge the support and funding from Monash University Malaysia and Ministry of Higher Education, Malaysia under the Grant No: FRGS/1/2013/SG02/MUSM/02/1.

REFERENCES

Basden, A. G., Morris, T. J., Gratadour, D. & Gendron, E., 2015. Sensitivity improvements for Shack-Hartmann wavefront sensors using total variation minimization. *Monthly Notices of the Royal Astronomical Society,* Volume 449, pp. 3537-3542.

Candes, E. J. & Romberg, J., 2005. Quantitative Robust Uncertainty Principles and Optimally Sparse Decompositions. *Classical Analysis and ODEs,* pp. 1-25.

Candes, E., Romberg, J. & Tao, T., 2006. Robust Uncertaunty Principles: Exact Signal Reconstruction from Highly Incomplete Frequency Information. *IEEE Transactions on Information Theory,* 52(2), pp. 489-509.

Dai, G.-M., 1994. *Modified Hartmann-Shack wavefront sensing and iterative wavefront reconstruction.* s.l., s.n.

Dalal, S., Klein, S., Barsky, B. & Corzine, J. C., 2001. Limitations to the Zernike representation of cornea and wavefront for post-refractive surgery eyes, (ARVO avstract). *Investigative Ophtalmology and Visual Science,* 42(4), p. S603.

Donoho, D. L., 2006. Compressed Sensing. *IEEE Transactions on Information Theory,* 52(4), pp. 1289-1306.

Guo, W. et al., 2013. Adaptive centroid-finding algorithm for freeform surface emasurements. *Applied Optics,* 52(10), pp. D75-D83.

Hosseini, M. & Michailovich, O. V., 2009. *Derivative Compressive Sampling with Application ti Phase Unwrapping.* Glasgow, s.n.

Lundstrom, L. & Unsbo, P., 2004. Unwrapping Hartmann-Shack Images from Highly Aberrated Eyes Using and Iterative B-Spline Based Extrapolation Method. *Optometry and Vision Science,* 18(5), pp. 383-388.

Noll, R. J., 1976. Zernike polynomials and atmospheric turbulence. *Optical Society of America,* Volume 66, pp. 207-211.

Platt, B. C. & Shack, R., 2001. History and Principles of Shack-Hartmann Wavefront Sensing. *Joirnal of Regractive Surgery,* Volume 17, pp. 573-577.

Polans, J., McNabb, R. P., Izatt, J. A. & Farsiu, S., 2014. Compressed Wavefront Sensing. *Optics Letters,* 39(5), pp. 1189-1192.

Rostami, M., Michailovich, O. & Wang, Z., 2012. Image Deblurring Using Derivative Compressed Sensing for Optical Imaging Application. *IEEE Transactions on Image Processing,* 21(7), pp. 3139-3149.

Schwiegerling, J. & Neal, D. R., 2005. Historical Development of the Shack-Hartmann Wavefront Sensor. *Robert Shannon and Roland Shack: Legends in Applied Optics,* pp. 132-139.

Yin, X., Li, X., Zhao, L. & Fang, Z., 2009. *Automatic centroid detection for Shack-Hartmann Wavefront sensor.* s.l., s.n.